BNL-107689-2015-JA

PCCP

PAPER

# Adsorbate-driven morphological changes on Cu(111) nano-pits

Cite this: DOI: 10.1039/c4cp05088f

K. Mudiyanselage,[ab] F. Xu,[ac] F. M. Hoffmann,[b] J. Hrbek,[a] I. Waluyo,[a] J. A. Boscoboinik[d] and D. J. Stacchiola*[a]

Received 4th November 2014,
Accepted 5th December 2014

DOI: 10.1039/c4cp05088f

www.rsc.org/pccp

Adsorbate-driven morphological changes of pitted-Cu(111) surfaces have been investigated following the adsorption and desorption of CO and H. The morphology of the pitted-Cu(111) surfaces, prepared by $Ar^+$ sputtering, exposed a few atomic layers deep nested hexagonal pits of diameters from 8 to 38 nm with steep step bundles. The roughness of pitted-Cu(111) surfaces can be healed by heating to 450–500 K in vacuum. Adsorption of CO on the pitted-Cu(111) surface leads to two infrared peaks at 2089–2090 and 2101–2105 $cm^{-1}$ for CO adsorbed on under-coordinated sites in addition to the peak at 2071 $cm^{-1}$ for CO adsorbed on atop sites of the close-packed Cu(111) surface. CO adsorbed on under-coordinated sites is thermally more stable than that of atop Cu(111) sites. Annealing of the CO-covered surface from 100 to 300 K leads to minor changes of the surface morphology. In contrast, annealing of a H covered surface to 300 K creates a smooth Cu(111) surface as deduced from infrared data of adsorbed CO and scanning tunnelling microscopy (STM) imaging. The observation of significant adsorbate-driven morphological changes with H is attributed to its stronger modification of the Cu(111) surface by the formation of a sub-surface hydride with a hexagonal structure, which relaxes into the healed Cu(111) surface upon hydrogen desorption. These morphological changes occur ~150 K below the temperature required for healing of the pitted-Cu(111) surface by annealing in vacuum. In contrast, the adsorption of CO, which only interacts with the top-most Cu layer and desorbs by 160 K, does not significantly change the morphology of the pitted-Cu(111) surface.

## A Introduction

Surface science studies are traditionally performed with well-annealed, "smooth" and stable surfaces and interactions/reactions of adsorbed species are investigated on coordinatively saturated surface-sites or atoms. However, in catalytically active surfaces, chemical reactions often occur at under-coordinated active-sites. Therefore, probing the interactions of adsorbed species with defect-sites or -surfaces is essential for the understanding of catalytic reactions. These defect sites are in general changing under reaction conditions and have been described as dynamic active-sites.[1] Isolating and investigating the stability of these catalytically active defect-sites is important in heterogeneous catalysis.

Low-energy ion bombardment, *e.g.* with $Ar^+$, introduces a wide variety of surface defects in the form of mounts and pits.[2] Even though the ion bombardment increases the roughness of a surface, its crystallinity is preserved.[1,3–5] There have been numerous studies on defective Cu, Au, Pt, Ni and Ag surfaces prepared by ion sputtering,[1,3–18] characterizing morphological changes due to ion sputtering as well as the interactions of adsorbates with defective surfaces. The roughness of defective surfaces can be removed by heating the sample to sufficiently high temperatures, so that the mobility of atoms is high enough to reach their thermodynamic equilibrium and thus flatten the surface. In addition, adsorbate-driven morphological changes have been observed on sputtered Au(111) following the adsorption of CO under ultra-high vacuum (UHV) conditions at low temperatures[1] as well as high pressures[9] up to 1 mbar at around 300 K. Weakly interacting adsorbates can be stabilized on defective surfaces, *e.g.* as shown for ethene adsorption on defective Cu(111) compared to its adsorption on smooth Cu(111).[10]

Copper-based catalysts are used for various important catalytic processes involving CO and $H_2$, such as the water gas shift reaction,[19–22] the hydrogenation of CO for the synthesis of methanol,[23] and CO oxidation.[24–26] Copper nanoparticles used as industrial catalysts expose many surface defect sites compared with the flat Cu(111) surface. Therefore, investigating the adsorption of CO and H on defect-sites of Cu(111) and monitoring the dynamic morphological changes during adsorption–desorption processes is essential for the mechanistic understanding of

[a] Chemistry Department, Brookhaven National Laboratory, Upton, NY 11973, USA. E-mail: djs@bnl.gov
[b] Department of Science, BMCC-CUNY, New York, NY 10007, USA
[c] Chemistry Department, State University of New York (SUNY), Stony Brook, NY 11794, USA
[d] Center for Functional Nanomaterials, Brookhaven National Laboratory, Upton, NY 11973, USA

catalytic reactions under reaction conditions. CO is also widely used as a probe molecule to characterize catalytic surfaces due to its very intense IR signal and its sensitivity to changes in local environments and adsorption sites, and we use it in this study to probe surface morphological changes on Cu(111). We show that the presence of hydrogen atoms induces relatively strong morphological changes upon annealing to 300 K in contrast to the adsorption of CO. These adsorbate-driven morphological changes occur ~150 K below the temperature required to remove the roughness of the pitted-Cu(111) by annealing in vacuum.

## B Experimental

Scanning tunnelling microscopy (STM) experiments were performed using a SPECS™ Aarhus HT-NAP STM, which contains an ambient pressure (AP) cell housed in a UHV chamber.[27] The Cu(111) single crystal was cleaned by $Ar^+$ sputtering and 800 K annealing cycles. The pitted-Cu(111) surfaces were prepared by sputtering the surface at normal incidence at 300 K with Ar ion energy = 1 keV and current density ~1 μA $cm^{-2}$. Infrared reflection absorption spectroscopy (IRRAS) experiments were performed in a combined UHV surface analysis chamber and elevated-pressure reactor/IRRAS cell system.[1] The surface analysis chamber is equipped with Auger electron spectroscopy (AES), low energy electron diffraction (LEED), and temperature programmed desorption (TPD) techniques. The elevated-pressure cell is coupled to a commercial Fourier transform infrared (FT-IR) spectrometer (Bruker, IFS 66v/S) for IRRAS experiments. The Cu(111) single crystal was held tightly using a Ta loop embedded in a groove machined around the crystal edge. The Ta loop was attached directly to the manipulator feed-through which was used for both mechanical support and heating/cooling. The sample temperature was measured by a K-type thermocouple attached to the top edge of the crystal. The sample was exposed to CO by backfilling the IRRAS cell *via* a precision leak valve. The surface was exposed to atomic hydrogen at normal incidence from an atomic hydrogen source (Omicron "EFM H") mounted in line-of sight of the crystal.[28] Molecular hydrogen was introduced with a leak valve at the flange end of the atomic hydrogen source and pumped through the UHV chamber. During atomic hydrogen exposure, the molecular hydrogen pressure was typically kept at $1 \times 10^{-7}$ Torr. IRRA spectra were collected at 4 $cm^{-1}$ resolution using a grazing angle of approximately 85° to the surface normal. All the IR spectra collected were referenced to a background spectrum acquired from the pitted-Cu(111) sample prior to CO or H adsorption. AES spectra of the surfaces before AP experiments showed no measurable presence of oxygen or carbon on the surface, and a small amount (~1%) of carbon after the AP experiments.

## C Results and discussion

Fig. 1A shows the STM image of a pitted-Cu(111) surface obtained after brief sputtering of a smooth-Cu(111) surface for 1 minute at 300 K. After sputtering, the Cu(111) surface was covered mainly with hexagonal pits with a diameter from 8 to 38 nm. Depending on the sputtering parameters, one layer deep pits develop first followed by pits several layers deep with narrow (steep) steps, as shown by the line scan in Fig. 1B. After extended sputtering the ion bombarded surfaces reach dynamic equilibrium with characteristic size, depth and density of nested pits.[4,6,7,29–32]

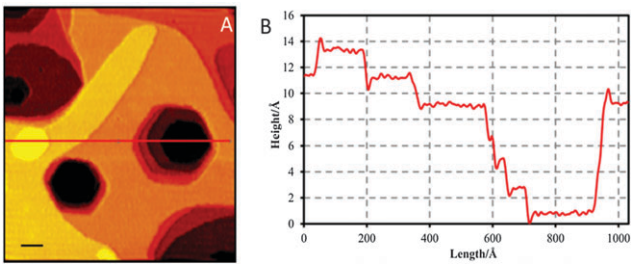


Fig. 1 Surface topography of pitted-Cu(111) under UHV conditions. (A) An STM image at 300 K. The red line indicates a line scan shown in (B). Scale bar: 10 nm, scanning current: 0.67 nA; scanning voltage: 1.63 V.

Fig. 2 shows a series of IRRA spectra obtained during the adsorption and desorption of CO on the pitted-Cu(111) surface, which was prepared by sputtering the flat Cu(111) surface for 5 minutes at 300 K. Fig. 2A shows IRRA spectra collected during the adsorption of CO while cooling the sample from 200 K to 100 K in CO background (~$2.0 \times 10^{-9}$ Torr). The vibrational spectrum obtained at 180 K (second from the top) shows two peaks at 2090 and 2105 $cm^{-1}$ indicating the presence of two different adsorption sites. With a decrease of the temperature to 150 K (fifth from the top), a third peak appears at 2071 $cm^{-1}$ and the peak at 2105 $cm^{-1}$ shifts to 2100 $cm^{-1}$. The peak at 2071 $cm^{-1}$ can be assigned to CO on the regular sites of well-ordered Cu(111) surface as reported previously.[33,34] Further decrease in temperature leads to increasing intensities of peaks at 2071 and 2100 $cm^{-1}$ and the disappearance of the peak at 2090 $cm^{-1}$ as it is masked by the intense peaks at 2071 and 2100 $cm^{-1}$. The peaks observed at 2090 and 2105 $cm^{-1}$ can be assigned to CO adsorbed on under-coordinated defect sites

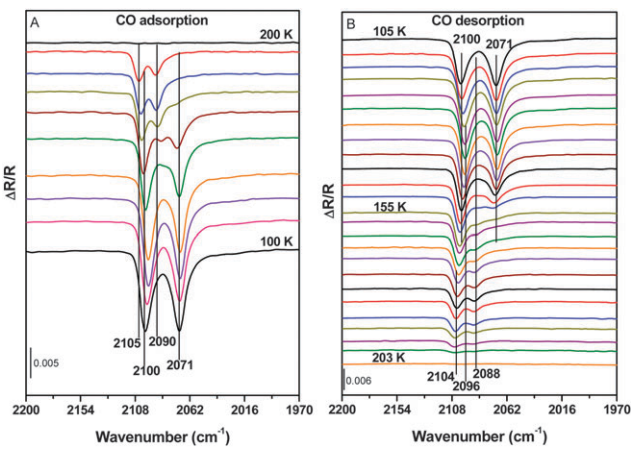


Fig. 2 (A) IRRA spectra for the adsorption of CO while cooling down the sample from 200 K in CO (~$2.0 \times 10^{-9}$ Torr) on the pitted-Cu(111) prepared by sputtering the Cu(111) surface at 300 K for 5 min. (B) IRRA spectra collected during the annealing of the CO saturated pitted Cu(111) surface shown in (A) (bottom spectrum) from 150 to 203 K with 0.1 K $s^{-1}$ heating rate.


This journal is © the Owner Societies 2014

Table 1 CO stretch IR frequency on copper sites

| Sample | C.N. | Wavenumber ($cm^{-1}$) | Ref. |
|---|---|---|---|
| Cu(111) | 9 | 2071 | 34–36 |
| Cu(100) | 8 | 2085 | 35, 37 |
| Cu(110) | 7 | 2091 | 35, 37 |
| Cu(211) | 6 | 2100 | 37 |
| $Cu/SiO_2/Mo(110)$ | Particle | 2106 | 38 |

formed as a result of the pits generated by $Ar^+$ sputtering as shown by the STM image in Fig. 1.

Table 1 summarizes the IRRAS data reported in the literature for the adsorption of CO on various surfaces with the topmost Cu atoms having different coordination numbers. The peak observed at ~2090 $cm^{-1}$ can be attributed to adsorbed CO on Cu sites with a coordination number between 7 and 8. This agrees with the reported formation of (100)-microfacet steps on shallow Cu(111) pits.[39,40] The peaks at 2105–2100 $cm^{-1}$ can be assigned to adsorbed CO on Cu sites with a coordination number of 6, which could be located at kinks/corners on the steps and on the facets created by the narrow (steep) steps shown in Fig. 1, which could lead to under-coordinated adsorption sites similar to the high index Cu(211) surface.

Fig. 2B shows a series of IRRA spectra collected during annealing of the CO covered surface in Fig. 2A (bottom spectrum) from 105 to 203 K with a 0.1 K $s^{-1}$ heating rate. The peak at 2071 $cm^{-1}$ for adsorbed CO on top sites of Cu(111) disappears due to the desorption of CO at 155 K.[34] With a further increase in the temperature, the intensity of the peak at 2088 $cm^{-1}$ initially increases slightly with a simultaneous decrease of the intensity of the peak at ~2104 $cm^{-1}$ and then both peaks disappear completely at 203 K. These data clearly show that the adsorbed CO on the under-coordinated Cu sites are more strongly bound than that on regular sites on Cu(111).

Fig. 3 shows a series of IRRA spectra collected following the adsorption of CO on several pitted-Cu(111) surfaces prepared by different sputtering times. The spectrum obtained after the adsorption of CO on a surface sputtered for 1 minute shows only a slightly broadened peak compared with the spectrum obtained from smooth Cu(111) (top spectrum). CO adsorbed on the surface prepared by sputtering for 2 minutes shows a peak at 2101 $cm^{-1}$ in addition to the peak at 2071 $cm^{-1}$ for CO on regular Cu(111) sites. With increasing sputtering time, the intensity of the peak at 2101 $cm^{-1}$ increases whereas the intensity of the peak at 2071 $cm^{-1}$ decreases simultaneously. The spectrum obtained from the surface prepared by sputtering for 11 minutes shows two peaks at 2071 and 2101 $cm^{-1}$ with equal intensities. In the system prepared by sputtering for 21 minutes, the intensity of the peak at 2101 $cm^{-1}$ is higher than that of the peak at 2071 $cm^{-1}$. These results clearly show the expected increase of the density of defect sites with increasing sputtering time, which results in an increase in the total steps length of the pits.

Fig. 4 shows the IRRA spectra obtained from a pitted-Cu(111) surface followed by annealing the sample to the specified temperatures and subsequent adsorption of CO at 100 K. First the Cu(111) sample sputtered at 300 K for 5 minutes

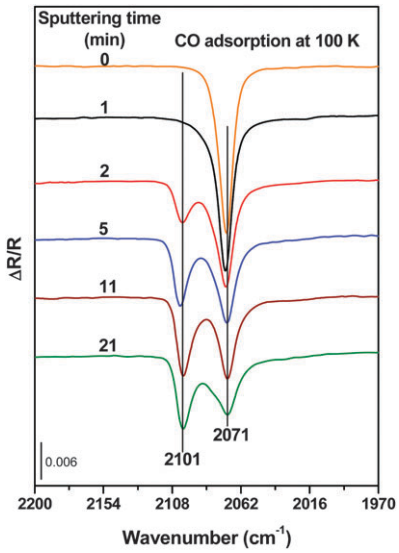


Fig. 3 IRRA spectra obtained for the saturation coverage of CO on pitted-Cu(111) surfaces as a function of sputtered time. The spectrum obtained for saturation coverage of CO on smooth Cu(111) at 100 K is also displayed for comparison (top spectrum).

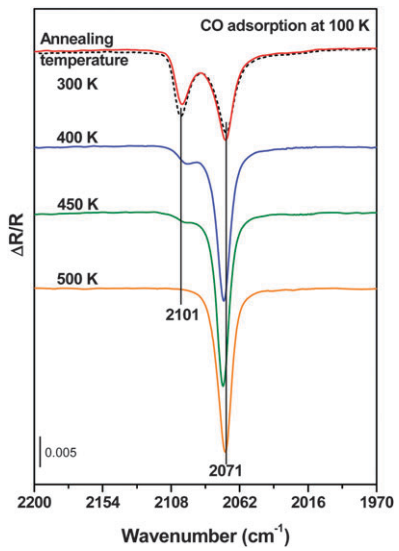


Fig. 4 IRRA spectra obtained following the adsorption of CO on pitted-Cu(111) at 100 K and re-adsorption of CO at 100 K after annealing to the specified temperatures (heating rate 2 K $s^{-1}$). The dashed-line spectrum was obtained following the first adsorption of CO on the pitted-Cu(111) surface at 100 K.

was cooled down and exposed to CO at 100 K. The spectrum collected at 100 K shows two peaks at 2071 and 2101 $cm^{-1}$ (top dashed-line spectrum in Fig. 4). After annealing of this CO covered surface to 300 K (note that adsorbed CO desorbs completely at 200 K), the sample was re-cooled and exposed to CO at 100 K. This second CO adsorption spectrum (Fig. 4, top solid-line spectrum) is similar to that observed after the first CO adsorption with only slight intensity changes. These results indicate that CO adsorption–desorption and annealing to 300 K

does not lead to significant morphological changes of the sputtered surface probed by CO adsorption. In contrast, on the pitted-Au(111) surface, repeated adsorption and desorption of CO resulted in drastic morphological changes of the surface.[1] Annealing to 400 K of the pitted-Cu(111) surface leads to an almost complete loss of defect sites, as shown by the strong reduction in intensity of the 2101 $cm^{-1}$ peak (third spectrum from the top in Fig. 4). The loss of defect sites is accompanied by an increase in intensity of the 2071 $cm^{-1}$ peak for CO on regular Cu(111) sites by more than a factor of two. A very weak feature remains at 2101 $cm^{-1}$ for CO adsorbed on defect sites after annealing to 450 K and it completely disappears after annealing to 500 K. At this temperature the surface mobility and intra-layer transport is high enough for the complete removal of the surface roughness/defects.[4]

Fig. 5 shows AP-IRRA spectra obtained during the exposure of pitted-Cu(111) to CO at the specified pressures at 300 K. At 8 mTorr pressure, two smaller peaks at 2103 and 2089 $cm^{-1}$, superimposed on a broad double band (due to gas phase CO), are observed. The two peaks at 2103 and 2089 $cm^{-1}$ are characteristic for CO adsorbed on defect sites similar to the results obtained at 100 K under UHV conditions. As the pressure increases, the intensity of the peak at 2103 $cm^{-1}$ increases, and the weak peak at 2089 $cm^{-1}$ disappears. At 600 mTorr pressure, a peak for (weaker bound) CO on regular Cu(111) sites appears at 2070 $cm^{-1}$ and grows with increasing pressure. The strong intensity of the 2103 $cm^{-1}$ peak demonstrates that defect sites are stable at 300 K under 1.0 Torr of CO pressure. The loss of the defect sites is observed only after annealing to 450 K, as shown in the bottom spectrum of Fig. 5, which shows the loss of the 2103 $cm^{-1}$ peak and a simultaneous intensity increase of the 2070 $cm^{-1}$ peak. The presence of only one peak at 2070 $cm^{-1}$ for CO on regular sites on Cu(111) indicates that a well-ordered smooth surface formed during annealing to 450 K in 1.0 Torr.

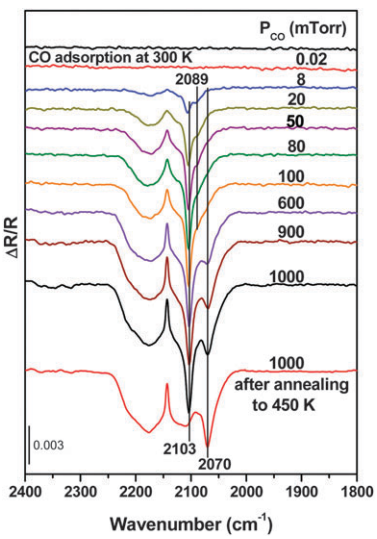


Fig. 5 AP-IRRA spectra obtained during the exposure of pitted-Cu(111) to CO at 300 K. A series of IR spectra were collected as a function of CO pressure. All the spectra were collected under CO gas at the specified pressure at 300 K. The bottom spectrum was obtained at 300 K after annealing to 450 K in 1.0 Torr of CO. The pitted-Cu(111) system was prepared by sputtering the Cu(111) surface for 4 min at 300 K.

These results show a higher stability for the pitted-Cu(111) surface under these reaction conditions (1 Torr at 300 K) than the pitted-Au(111) surface,[9] where CO exposure under comparable conditions (0.75 Torr at 300 K) resulted in massive atomic movements on the pitted-Au(111) surface leading to its smoothing and consequently to a lower CO binding capacity.[9] Atomic movements on the pitted-Au(111) surface have been observed even under much milder conditions at temperatures below 180 K and very low CO pressures ($5 \times 10^{-9}$ Torr), where weakly adsorbed CO induced irreversible morphological changes of the surface.[1]

In order to investigate the effects of ambient pressure CO on the morphology of the pitted surface, AP-STM images were obtained before exposure to CO and under 700 mTorr of CO at 300 K as shown in Fig. 6. The comparison between the images in Fig. 6 shows that the original hexagonal shape of the pits under UHV, shown in Fig. 6A, is rounded off when exposed to CO, as shown in Fig. 6B during CO exposure, and the edges of the pits are decorated by nano-sized particles, similar to the case of Au(111).[1] In addition, a triangular-shaped step edge in the image obtained before exposure to CO is also smoothened. The overall area of pits was maintained.

The fact that Cu(111) is active for the hydrogenation of $CO_2$, at temperatures between 500–600 K and $H_2$ pressures ~4.5 atm,[41] indicates that it can dissociate $H_2$ at elevated temperature and pressure. But dissociation of molecular hydrogen could not be detected at room temperature (300 K) even after exposure of the pitted surface to 1.5 Torr of $H_2$. Therefore, in order to investigate the effect of hydrogen on the morphology of the pitted surface, we decided to expose the nano-pitted surfaces to atomic hydrogen.

Fig. 7 shows IRRA spectra for the adsorption of H on pitted-Cu(111) together with spectra of adsorbed CO to characterize the surface before and after the adsorption of H.

The top spectrum (a) was obtained for the saturation coverage of CO on pitted-Cu(111) at 100 K. Characteristic of the pitted-Cu(111) surface, we observe two peaks at 2071 and 2099 $cm^{-1}$ for

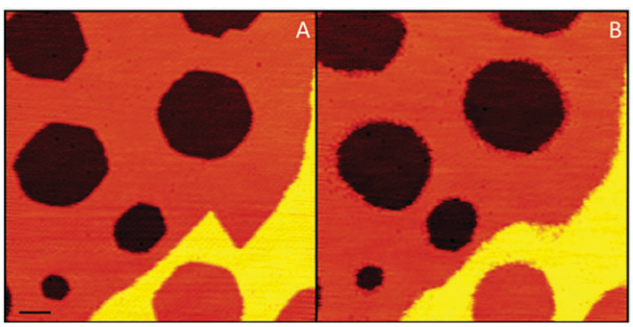


Fig. 6 AP-STM images of pitted-Cu(111) at room temperature. (A) Pitted-Cu(111) surface with one layer deep shallow hexagonal pits, and (B) same place as (A) but after 0.9 min exposure to 700 mTorr CO. The image was scanned under CO pressure. Scale bar = 10 nm. Scanning conditions: 0.64 nA, 1.53 V, scanning from bottom to top. (The pitted-Cu(111) surface was prepared by 30 s gentle sputtering at ~360 K with 0.50 keV source power and 0.8 μA target current.)


This journal is © the Owner Societies 2014

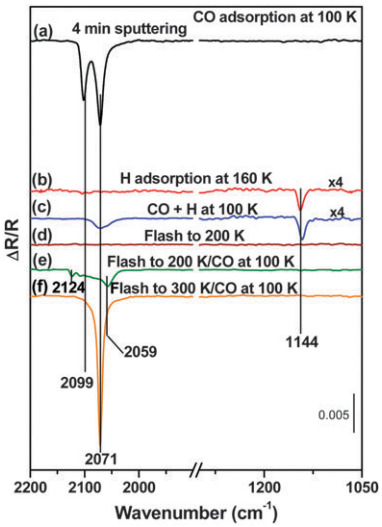


Fig. 7 IRRA spectra collected: (a) after saturation coverage of CO on pitted-Cu(111) at 100 K; (b) after adsorption of saturated coverage of H at 160 K; (c) co-adsorption of CO on the system in (b) at 100 K; (d) after annealing of the system in (c) to 200 K (spectrum was collected at 200 K); (e) after re-adsorption of CO on the system in (d) at 100 K; (f) after the annealing of the system in (e) to 300 K followed by re-cooling and the re-adsorption of CO at 100 K.

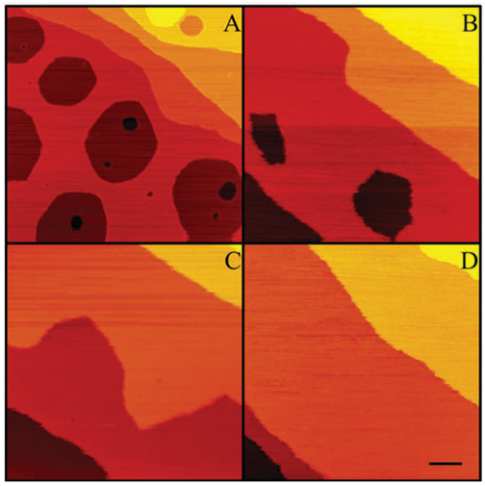


Fig. 8 STM images of the pitted-Cu(111) surface and its topography before and after atomic hydrogen treatment at 300 K. (A) Pitted-Cu(111) surface as prepared; exposure to atomic hydrogen for (B) 5 min, (C) 10 min and (D) 20 min. Scale bar = 15 nm. 0.51 nA, 1.00 V, scanning from bottom to top.

CO adsorbed on regular and defect copper sites, respectively. After removing CO by annealing to 160 K, this surface was then exposed to atomic H at 160 K. A peak observed at 1144 $cm^{-1}$ as shown in spectrum (b) for the adsorbed Cu–H was reported previously for H adsorbed on smooth Cu(111).[28] The spectrum (c) was obtained after exposure of pitted-Cu(111) to H at 160 K and subsequent exposure to CO at 100 K. Spectrum (c) shows a broad and weak peak for adsorbed CO at 2071 $cm^{-1}$ in addition to the peak at ~1141 $cm^{-1}$ for adsorbed H. The CO peak intensity is strongly reduced compared to that of a saturation coverage of CO on pitted-Cu(111) (spectrum (a)). The spectrum (c) is characteristic of co-adsorbed CO and H, as it shows that the presence of H suppresses the adsorption of CO.[28] The spectrum obtained after similar preparation using flat Cu(111) shows a slightly red shifted peaks at 1132 and 2059 $cm^{-1}$ for adsorbed H and CO, respectively, as reported previously.[28] Annealing of the system in (c) to 200 K results in the complete desorption of CO and the disappearance of the surface Cu–H vibration peak as shown in spectrum (d) due to the migration of H to sub-surface sites, leading to the formation of a thin copper hydride (CuH) layer as described earlier on Cu(111) surfaces.[28] Spectrum (e) was obtained after re-cooling to 100 K and re-adsorption of CO on top of the CuH surface. The Cu–H peak at 1141 $cm^{-1}$ has completely disappeared, but CO adsorption is still strongly suppressed as indicated by the reduced intensity of the C–O peak at 2059 $cm^{-1}$. This 2059 $cm^{-1}$ peak is also accompanied by several small peaks at higher frequencies (2095–2124 $cm^{-1}$) similar to previously reported results on the CuH layer formed on the annealed Cu(111).[28] The bottom spectrum (f) in Fig. 7, which shows an intense peak for adsorbed CO on regular Cu(111) sites at 2071 $cm^{-1}$, was obtained after annealing the system in (e) to 300 K, where all the hydrogen has desorbed from the surface, as previously observed by TPD,[28] and re-adsorption of CO at 100 K.

To further corroborate the healing of pitted-Cu(111) surfaces by adsorption–desorption of hydrogen, we carried out STM studies. Fig. 8 shows the process of healing the pitted-Cu(111) surface by exposure to atomic hydrogen. After gentle $Ar^+$ sputtering, a Cu(111) surface is shown with shallow hexagonal pits (Fig. 8A). After 5 min exposure to atomic hydrogen at 300 K, the pits on the surface are partially healed (Fig. 8B). This trend continues with further exposure to atomic hydrogen (Fig. 8C). After 20 min atomic hydrogen treatment, the pitted-Cu(111) surface is completely healed (Fig. 8D). We also carried out control experiments where a similar pitted-Cu(111) surface was scanned in vacuum at 300 K for longer time (~4 hours) than used for the hydrogen healing experiment described above. Mobility of the pits was observed under vacuum, similar to the effect reported on Ag(111),[33] but pits were not healed and remained present on the surface at all times.

In contrast with earlier work on nano-pitted Au(111) surfaces, the current results show that annealing of a CO covered pitted-Cu(111) surface to 300 K or its exposure to ambient pressure CO at 300 K does not lead to significant morphological changes of the pitted surface as shown by Fig. 4 and 5. But if atomic hydrogen is provided to a rough Cu surface it can fully heal it. Annealing of a H covered pitted-Cu(111) surface to 300 K, or its exposure to atomic hydrogen at 300 K leads to significant morphological changes resulting in a flat Cu(111) surface.

In order to elucidate the effect of subsurface hydrogen on the morphology of the pitted Cu surface, we can first refer to the interaction of hydrogen with bulk copper. Bulk copper hydride (CuH) has been shown to form a hexagonal structure.[42] It was recently reported that the absorption of atomic H on Cu(100) at low temperatures leads to the formation of a metastable surface hydride, which induces the reconstruction of the originally square surface into a structure with an approximated hexagonal

cell.[43] We can then explain the reconstruction of our heterogeneous nano-pitted Cu(111) surface by the formation of a thin surface hydride with hexagonal structure, which upon desorption of the hydrogen fully relaxes to the hexagonal structure of the bulk crystal Cu(111). This explanation could also help us to understand the reconstruction of copper nanoparticles supported on oxide powder catalysts under reaction conditions.[44] Based on *in situ* environmental transmission microscopy (E-TEM) experiments at temperatures used for methanol synthesis and the WGS reaction ($\sim$220 °C), it was reported that Cu/ZnO catalysts present a higher fraction of Cu(111) facets in the presence of $H_2$ than under a mixture of $H_2$ and $H_2O$ under the same total pressure. The result was explained by the possible adsorption of water molecules on the surface of the copper nanoparticles and the stabilization of (110) and (100) facets. Since water adsorption energies on metals including Cu, either molecular or dissociative,[45] are small and more than 1 eV weaker than the absorption energies of hydrogen in hydrides,[46] we can now offer an alternative explanation based on our current results. The preponderance of (111) facets on Cu nanoparticles in the presence of higher partial hydrogen pressures can be related to the dynamic formation of small metastable CuH domains and their conversion to stable Cu(111) facets. This in turn can influence the catalytic activity of the reconstructed nanoparticles in hydrogenation reactions such as the methanol synthesis.

## Conclusions

After $Ar^+$ sputtering, Cu(111) surfaces were covered mainly with hexagonal pits of diameter from 8 to 38 nm. The small pits sit inside of bigger ones, forming sharp step bundles. In addition to pits, some hexagonal islands were also observed on terraces. The roughness of the pitted-Cu(111) surface can be removed by annealing in UHV to 450–500 K. Adsorption of CO on the pitted-Cu(111) surface shows two peaks at 2089–2090 and 2101–2105 $cm^{-1}$ for adsorbed CO on under-coordinated sites and a peak at 2071 $cm^{-1}$ for CO on regular Cu(111) sites. Adsorbed CO on defect sites is thermally more stable than that on regular Cu(111) sites. Annealing of the CO adsorbed pitted-Cu(111) surface at 100 K to 300 K or exposing of the pitted-Cu(111) surface to 1.0 Torr of CO at 300 K does not lead to significant morphological changes of the rough surface to remove defect sites. In contrast, the adsorption of atomic hydrogen on the pitted-Cu(111) surface at 160 K followed by annealing to 300 K to desorb H or exposing the pitted-Cu(111) surface to atomic hydrogen at 300 K completely reconstructs the surface leading to a smooth Cu(111) sample. This adsorbate-driven morphological changes occur $\sim$150 K below the temperature required to remove the roughness of the pitted-Cu(111) by annealing in vacuum. The observation of the drastic adsorbate-driven morphological changes with H is attributed to the formation of a sub-surface hydride with an hexagonal structure, which relaxes into the healed Cu(111) surface upon hydrogen desorption. In contrast, the adsorption of CO, which only interacts with the top-most Cu layer and desorbs by 160 K, does not significantly change the defect sites of the pitted-Cu(111) surface. These results highlight once more the importance of investigating the properties of the adsorption sites in the presence of adsorbates or under reaction conditions to identify dynamic active sites.

## Acknowledgements

This work was carried out at the Chemistry Department, Center for Functional Nanomaterials and National Synchrotron Light Source, Brookhaven National Laboratory, under Contract No. DE-AC02-98CH10886 with the U.S. Department of Energy, Office of Science, and supported by its Division of Chemical Sciences, Geosciences, and Biosciences within the Office of Basic Energy Sciences.

## Notes and references

1 J. Hrbek, F. M. Hoffmann, J. B. Park, P. Liu, D. Stacchiola, Y. S. Hoo, S. Ma, A. Nambu, J. A. Rodriguez and M. G. White, *J. Am. Chem. Soc.*, 2008, **130**, 17272–17273.
2 W. L. Chan and E. Chason, *J. Appl. Phys.*, 2007, **101**, 121301.
3 J. C. Girard, Y. Samson, S. Gauthier, S. Rousset and J. Klein, *Surf. Sci.*, 1994, **302**, 73–80.
4 J. Naumann, J. Osing, A. J. Quinn and I. V. Shvets, *Surf. Sci.*, 1997, **388**, 212–219.
5 M. Ritter, M. Stindtmann, M. Farle and K. Baberschke, *Surf. Sci.*, 1996, **348**, 243–252.
6 A. C. Bose and M. Yoshitake, *Appl. Surf. Sci.*, 2005, **241**, 174–178.
7 C. A. Lang, C. F. Quate and J. Nogami, *Appl. Phys. Lett.*, 1991, **59**, 1696–1698.
8 G. Costantini, S. Rusponi, R. Gianotti, C. Boragno and U. Valbusa, *Surf. Sci.*, 1998, **416**, 245–254.
9 Z. Paszti, O. Hakkel, T. Keszthelyi, A. Berko, N. Balazs, I. Bako and L. Guczi, *Langmuir*, 2010, **26**, 16312–16324.
10 O. Skibbe, D. Vogel, M. Binder, A. Pucci, T. Kravchuk, L. Vattuone, V. Venugopal, A. Kokalj and M. Rocca, *J. Chem. Phys.*, 2009, **131**. Q3
11 D. Heskett, D. DePietro, G. Sabatino and M. Tammaro, *Surf. Sci.*, 2002, **513**, 405–411.
12 J. Bremer, J. K. Hansen and O. Hunderi, *Surf. Sci.*, 1999, **436**, L735–L739.
13 D. W. Moon, Y. H. Ha, H. K. Kim, K. J. Kim, H. S. Kim, J. Y. Lee and S. Kim, *Appl. Surf. Sci.*, 1999, **150**, 235–243.
14 M. S. Hoogeman, M. A. J. Klik, R. van Gastel and J. W. M. Frenkens, *J. Phys.: Condens. Matter*, 1999, **11**, 4349–4365.
15 S. Rusponi, G. Costantini, C. Boragno and U. Valbusa, *Phys. Rev. Lett.*, 1998, **81**, 2735–2738.
16 G. Costantini, S. Rusponi, F. B. de Mongeot, C. Boragno and U. Valbusa, *J. Phys.: Condens. Matter*, 2001, **13**, 5875–5891.
17 S. Rusponi, G. Costantini, C. Boragno and U. Valbusa, *Phys. Rev. Lett.*, 1998, **81**, 4184–4187.
18 S. Rusponi, G. Costantini, C. Boragno and U. Valbusa, *Phys. Low-Dimens. Struct.*, 1999, **5–6**, 95–103. Q4

 This journal is © the Owner Societies 2014

19 D. S. Newsome, *Catal. Rev.: Sci. Eng.*, 1980, **21**, 275–318.
20 J. A. Rodriguez, J. Graciani, J. Evans, J. B. Park, F. Yang, D. Stacchiola, S. D. Senanayake, S. Ma, M. Pérez, P. Liu, J. F. Sanz and J. Hrbek, *Angew. Chem., Int. Ed.*, 2009, **48**, 8047–8050.
21 J. B. Park, J. Graciani, J. Evans, D. Stacchiola, S. D. Senanayake, L. Barrio, P. Liu, J. F. Sanz, J. Hrbek and J. A. Rodriguez, *J. Am. Chem. Soc.*, 2010, **132**, 356–363.
22 K. Mudiyanselage, S. D. Senanayake, L. Feria, S. Kundu, A. E. Baber, J. Graciani, A. B. Vidal, S. Agnoli, J. Evans, R. Chang, S. Axnanda, Z. Liu, J. F. Sanz, P. Liu, J. A. Rodriguez and D. J. Stacchiola, *Angew. Chem., Int. Ed.*, 2013, **52**, 5101–5105.
23 K. Klier, in *Advances in Catalysis*, ed. H. P. D. D. Eley and B. W. Paul, Academic Press, 1982, vol. 31, pp. 243–313.
24 S. D. Senanayake, D. Stacchiola and J. A. Rodriguez, *Acc. Chem. Res.*, 2013.
25 F. Yang, J. Graciani, J. Evans, P. Liu, J. Hrbek, J. F. Sanz and J. A. Rodriguez, *J. Am. Chem. Soc.*, 2011, **133**, 3444–3451.
26 F. Xu, K. Mudiyanselage, A. E. Baber, M. Soldemo, J. Weissenrieder, M. G. White and D. J. Stacchiola, *J. Phys. Chem. C*, 2014, **118**, 15902–15909.
27 A. E. Baber, F. Xu, F. Dvorak, K. Mudiyanselage, M. Soldemo, J. Weissenrieder, S. D. Senanayake, J. T. Sadowski, J. A. Rodriguez, V. Matolín, M. G. White and D. J. Stacchiola, *J. Am. Chem. Soc.*, 2013, **135**, 16781–16784.
28 K. Mudiyanselage, Y. Yang, F. M. Hoffmann, O. J. Furlong, J. Hrbek, M. G. White, P. Liu and D. J. Stacchiola, *J. Chem. Phys.*, 2013, **139**, 044712.
29 T. Michely and G. Comsa, *Surf. Sci.*, 1991, **256**, 217–226.
30 T. Michely, K. H. Besocke and G. Comsa, *Surf. Sci.*, 1990, **230**, L135–L139.
31 K. Morgenstern, G. Rosenfeld, B. Poelsema and G. Comsa, *Phys. Rev. Lett.*, 1995, **74**, 2058–2061.
32 K. Morgenstern, G. Rosenfeld, E. Laegsgaard, F. Besenbacher and G. Comsa, *Phys. Rev. Lett.*, 1998, **80**, 556–559.
33 R. Raval, S. F. Parker, M. E. Pemble, P. Hollins, J. Pritchard and M. A. Chesters, *Surf. Sci.*, 1988, **203**, 353–377.
34 K. Mudiyanselage, A. Wei, F. Yang, P. Liu and J. D. Stacchiola, *Phys. Chem. Chem. Phys.*, 2013, **15**, 10726–10731.
35 T. Wadayama, K. Kubo, T. Yamashita, T. Tanabe and A. Hatta, *J. Phys. Chem. B*, 2003, **107**, 3768–3773.
36 P. Hollins and J. Pritchard, *Surf. Sci.*, 1979, **89**, 486–495.
37 J. Pritchard, T. Catterick and R. K. Gupta, *Surf. Sci.*, 1975, **53**, 1–20.
38 X. Xu, S. M. Vesecky, J. W. He and D. W. Goodman, *J. Vac. Sci. Technol., A*, 1993, **11**, 1930–1935.
39 P. J. Feibelman, *Phys. Rev. B: Condens. Matter Mater. Phys.*, 1999, **60**, 11118–11122.
40 G. S. Icking-Konert, M. Giesen and H. Ibach, *Surf. Sci.*, 1998, **398**, 37–48.
41 J. Graciani, K. Mudiyanselage, F. Xu, A. E. Baber, J. Evans, S. D. Senanayake, D. J. Stacchiola, P. Liu, J. Hrbek, J. Fernandez Sanz and J. A. Rodriguez, *Science*, 2014, **345**, 546–550.
42 J. A. Goedkoop and A. F. Andresen, *Acta Crystallogr.*, 1955, **8**, 118–119.
43 A. Hellman, K. Svensson and S. Andersson, *J. Phys. Chem. C*, 2014, **118**, 15773–15778.
44 P. L. Hansen, J. B. Wagner, S. Helveg, J. R. Rostrup-Nielsen, B. S. Clausen and H. Topsøe, *Science*, 2002, **295**, 2053–2055.
45 J. Ren and S. Meng, *Phys. Rev. B: Condens. Matter Mater. Phys.*, 2008, **77**, 054110.
46 J. Greeley and M. Mavrikakis, *J. Phys. Chem. B*, 2005, **109**, 3460–3471.